Journal of Magnetism and Its Applications, 1 (2) 2021, 40-45

http://www.jourmag.org/index.php/jma

Journal of Magnetism and Its Applications

Received December 27th 2021; received in revised January 10th 2022; accepted January 11th 2022

Research article

Effect of ZnO on the Nanostructure, Magnetic, and Optical Properties of Fe_2O_3/MWCNT/ZnO Nanocomposites

Dzurriyah Haibatus Shalihah[1], ST. Ulfawanti Intan Subadra[1]*, Nashikhudin[1], Munasir[2], Yuanita Amalia Hariyanto[3]

[1]Department of Physics, Faculty of Mathematics and Natural Sciences, Universitas Negeri Malang, Malang 65145, Indonesia
[2]Department of Physics, Faculty of Mathematics and Natural Science, Universitas Negeri Surabaya, Surabaya 60213, Indonesia
[3]Study Program of Pharmacy, Faculty of Mathematics and Natural Sciences, Universitas Sam Ratulangi, Manado 95115, Indonesia

Article info

Keywords:
Fe_2O_3/MWCNT/ZnO
Nanocomposite
Nanostructure
Magnetization
Bandgap

Abstract

Fe_2O_3/MWCNT/ZnO nanocomposites were successfully synthesized through the precipitation method. The synthesis was carried out through a variation of ZnO mass, with (Fe_2O_3/MWCNT):ZnO mass ratio of 1:0, 1:0.5, 1:1, 1:1.5, and 0:1. The XRD analysis results suggested that the nanocomposites were composed of two phases, namely Fe_2O_3 with centered hexagonal structure and ZnO with hexagonal wurtzite structure. The ZnO diffraction peak tended to increase following the increasing ZnO composition within the nanocomposites. The presence of MWCNT was confirmed by the FTIR results signifying the detection of C=C vibration at wavenumbers of 1631–1640 cm^{-1}. The crystallite size of Fe_2O_3 and ZnO was in the range of 30.97–31.12 nm and 30.46–35.64 nm, respectively. The nanocomposites were comprised of the spherical, tube, and sheet particles, representing Fe_2O_3, MWCNT, and ZnO, respectively, with particle size ranged from 33.97 nm to 55.19 nm. The nanocomposites were observed to present weak ferromagnetic, with a decrease in saturation magnetization value following the increase of ZnO composition. The optical properties of the nanocomposites tended to decrease as the increasing ZnO composition.

1. Introduction

Recently, a number of studies have developed composite-based technologies. This situation is induced by the composite's capability to present new characteristics while maintaining the authentic features of the constituent particles. This excellent feature has been proven to enhance the performance of the material's application in medical, technological, and military fields, such as the application as drug delivery system, antimicrobial agent, as well as sensor and microwave or radar absorbing material (MAM or RAM) [1]. Theoretically, the nanocomposite is comprised of two or more materials with combined characteristics from its constituent materials or even with new and better features [2]. Further, in recent decades, composite has been prepared in nano-sized or known as nanocomposite. Nano-sized particles carry better physical and chemical properties than bulk-sized particles [3]. Commonly, the nanocomposite is comprised of filler and matrix, in which the successfully inserted filler into the matrix results in a new characteristic that is distinct from its constituent material.

In recent years, studies have reported many nanocomposites that are consisted of magnetic and dielectric materials, such as Fe_3O_4 or Fe_2O_3 and carbon. Taufiq et al. have successfully fabricated Fe_3O_4 composited with activated carbon (AC) used as radar absorbing material (RAM) [4, 5]. Rahmawati *et al.* have composited Fe_3O_4 as magnetic material and multi-walled carbon nanotubes (MWCNT) as dielectric material for voltage sensors [6]. Aside from Fe_3O_4, one of the most developed magnetic materials is Fe_2O_3 because it is classified as the most stable material [7]. Besides, the Fe_2O_3 nanoparticle also carries unique features, such as an n-type semiconductor with a small bandgap of 2.1 eV [8] and corrosion resistance [9]. Therefore, the Fe_2O_3 nanoparticle has been massively applied as photocatalyst [10], sensor gas [11], and Li-ion battery [12].

In this study, the Fe_2O_3 performance is enhanced through combination with carbon material of MWCNT. This material was selected due to its great mechanical and thermal properties [13], wide surface area [14], low density [15], high dielectric loss [13], and conductive [16]. According to R. Leary and A. Westwood, a combination of Fe_2O_3 dan MWCNT can improve the performance of its application as a photocatalyst due to its chemical stability, extensive surface area, and high electron conductivity [17]. However, in some applications, such as RAM, antimicrobial, and gas sensors, the Fe_2O_3/MWCNT nanocomposite has not presented maximum performance. Therefore, this study also adds ZnO in the Fe_2O_3/MWCNT nanocomposite. Soplanit et al, have successfully combinated Fe_2O_3 with Fe_3O_4 and ZnO for antibacterial agent. The results showed that nanocomposites had good performance to inhibit bacterial growth [18].

ZnO nanoparticle is a semiconductor material with a high dielectric constant, stable toward heat, and excellent electrical conductivity [19]. In the biomedical field, ZnO carries a number of excellent features in a number of applications, such as antimicrobial and drug delivery agents [20], because of its non-allergic, non-toxic, and non-irritating characteristic [24, 25]. Besides, ZnO is also commonly used in sensors, photocatalysts, supercapacitors, and other applications due to its wide bandgap, light, low-cost, and easily produced [26, 27]. Wang et al. report that ZnO is capable of enhancing impedance matching in the application of RAM in the nanocomposite comprised of magnetic and dielectric material, obtaining a high reflection loss value caused by the high complex permittivity of this particle [25]. Therefore, this study develops Fe_2O_3/MWCNT/ZnO nanoparticles, as well as investigates the effects of ZnO mass within the nanostructure, magnetic, and optical properties of nanocomposites.

2. Experimental Methods

The synthesis of Fe_2O_3/MWCNT/ZnO nanocomposites was carried out using the precipitation method. It was started by the functionalization process with nitric acid [1, 6]. It was followed with ZnO preparation using the sol-gel method following the stages in our previous studies [20]. In the third step, the Fe_2O_3/MWCNT nanocomposite was prepared using 20 grams of $FeCl_3.6H_2O$ solved into 40 ml of distilled water, and stirred using a magnetic stirrer at 520 rpm. Further, 0.1 gram of functionalized MWCNT was added to the solution, followed

*Corresponding author
Email: intansubadra97@gmail.com

DOI: 10.53533/JMA.v1i2.16

by titration NH_4OH until pH 9, and one hour stirring. The reaction result was washed using distilled water until the neutral pH was obtained. The obtained deposit was dried at 100 °C temperature and calcined at 800 °C temperature for 1 hour. In the last phase of Fe_2O_3/MWCNT/ZnO nanocomposite preparation, the Fe_2O_3/MWCNT powder was dissolved into 50 mL distilled water using an ultrasonic bath for 30 minutes at room temperature. Further, the ZnO powder was added into the obtained solution and stirred for 30 minutes using a magnetic stirrer. The obtained solution was heated at 100 °C temperature for one hour to attain Fe_2O_3/MWCNT/ZnO nanocomposites in powder. This study used a variation of ZnO mass, with (Fe_2O_3/MWCNT):ZnO mass ratio of 1:0, 1:0.5, 1:1, 1:1.5, and 0:1, coded with Zn0, Zn1, Zn2, Zn3, and Zn4, respectively.

3. Results and Discussion

The diffraction pattern of Fe_2O_3/MWCNT/ZnO nanocomposites obtained from X-ray diffractometer characterization is illustrated in Figure 1. The ZnO diffraction pattern represents the Fe_2O_3/MWCNT diffraction pattern, in which the peaks are detected at 2θ 24.2°, 33.2°, 35.7°, 40.9°, 49.5°, 54.1°, 57.7°, 62.5°, and 64.2 ° which represent the miller planes of (0 1 2), (1 0 4), (1 1 0), (1 1 3), (0 2 4), (1 1 6), (0 1 8), (2 1 4), and (0 3 0), consecutively. The obtained results are linear with previous studies carried out by Lassoued *et al.* [26]. The absence of MWCNT functionalized is due to the low composition of MWCNT compared to the Fe_2O_3. Meanwhile, the diffraction pattern of ZnO nanoparticles is represented by the pattern of Zn4. The ZnO's peaks are observed at 31.8° (0 1 0), 34.5° (0 0 2), 36.3° (0 1 1), 47.6° (0 1 2), 56.7° (1 1 0), 62.9° (0 1 3), 66.5° (0 2 0), 68.1° (1 1 2), and 69.2° (0 2 1). Similar results have been reported in a previous works [20].

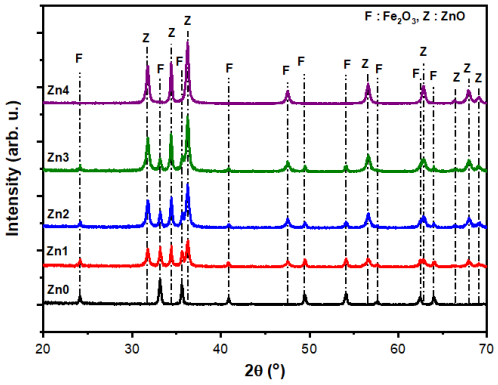

Fig. 1. X-ray diffraction patterns of the Fe_2O_3/MWCNT/ZnO nanocomposites

The success of Fe_2O_3/MWCNT/ZnO nanocomposite preparation is marked by the appearance of the Fe_2O_3 and ZnO peaks, with ZnO peaks that tend to increase in line with the increase of ZnO mass. A quantitative analysis was also carried out by comparing the experiment results with database AMCSD No. 0000143 for the Fe_2O_3 phase and AMCSD No. 0005203 for the ZnO phase. The analysis results show that Fe_2O_3 presents a centered hexagonal structure in rhombohedral with a space group of R-3c, while the ZnO has a hexagonal wurtzite structure. As presented in Table 1, the crystallite size of the composite ranges from 30.13–31.12 nm. Meanwhile, the crystallite size of ZnO nanoparticles tends to increase, from 30.46 nm to 35.64 nm, following the addition of ZnO within the nanocomposites. The increase in the crystal size of the ZnO nanoparticles was associated with higher and narrower diffraction peaks as the ZnO mass increased. According to the Scherer equation, a narrow diffraction peak results in a small FWHM value, so the larger the crystal size.

Table 1. Crystallite Size of the Fe_2O_3/MWCNT/ZnO nanocomposites

Sample	Crytallite Size (nm)	
	Fe_2O_3	ZnO
Zn0	31.12	-
Zn1	30.13	30.46
Zn2	30.08	32.54
Zn3	30.97	34.35
Zn4	-	35.64

The results of FTIR characterization are presented in Figure 2. Figure 2 shows that the primary transmittance peak of Fe_2O_3/MWCNT/ZnO nanocomposites is observed at wavenumbers of 400–567 cm^{-1}, representing the Fe-O vibration of the Fe_2O_3 [27], while the peak at 1631-1640 cm^{-1} represents the C=C bound vibration from the graphite, as the constituent of MWCNT [1]. Further, the ZnO vibration appeared at 561 cm^{-1}, showing the characteristic of Zn-O vibration [28]. Aside from those three primary vibrations of the Fe_2O_3/MWCNT/ZnO nanocomposites, other peaks are also observed, such as the C-H peak at a wavenumber of 904 cm^{-1}, which is the out of plane bending of the alkene group from the zinc acetate dehydrate [29, 30]. Besides, vibration from the COO bound is also detected at wavenumbers of 1375–1394 and 1541–1566 cm^{-1} [31]. This vibration appears as the result of functionalization on MWCNT. Furthermore, the O-H bound is also found at 3448 cm^{-1} from the water.

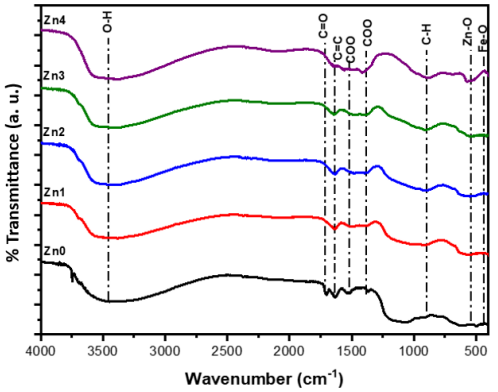

Fig. 2. FTIR Spectra of the Fe_2O_3/MWCNT/ZnO nanocomposites

The morphology of Fe_2O_3/MWCNT/ZnO nanocomposites was obtained from the SEM characterization, as presented in Figure 3. Figure 3 illustrates that the nanocomposite is comprised of spherical particle that tends to agglomerate and tube particle, representing the Fe_2O_3 and MWCNT, respectively. A similar result has also been reported by Rachmawati *et al.* [2]. After the addition of ZnO, the nanocomposite's agglomeration level tends to decrease. Meanwhile, the increase of ZnO mass escalates the amount of sheet constituent particles, such as the Zn4 morphology that tends to cover the spherical nanoparticles. The average diameter of the nanocomposite was also analyzed using a normal log function and the result of the diameter analysis is shown in Figure 4.

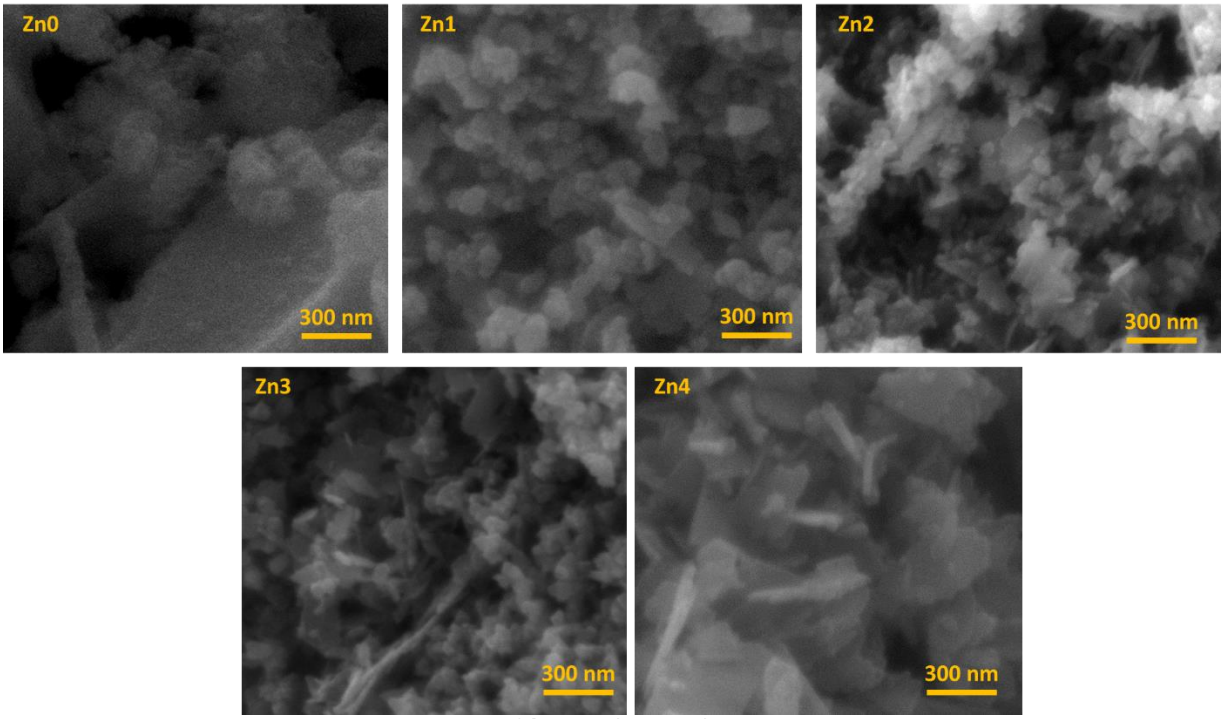

Fig. 3. SEM images of the Fe_2O_3/MWCNT/ZnO nanocomposites

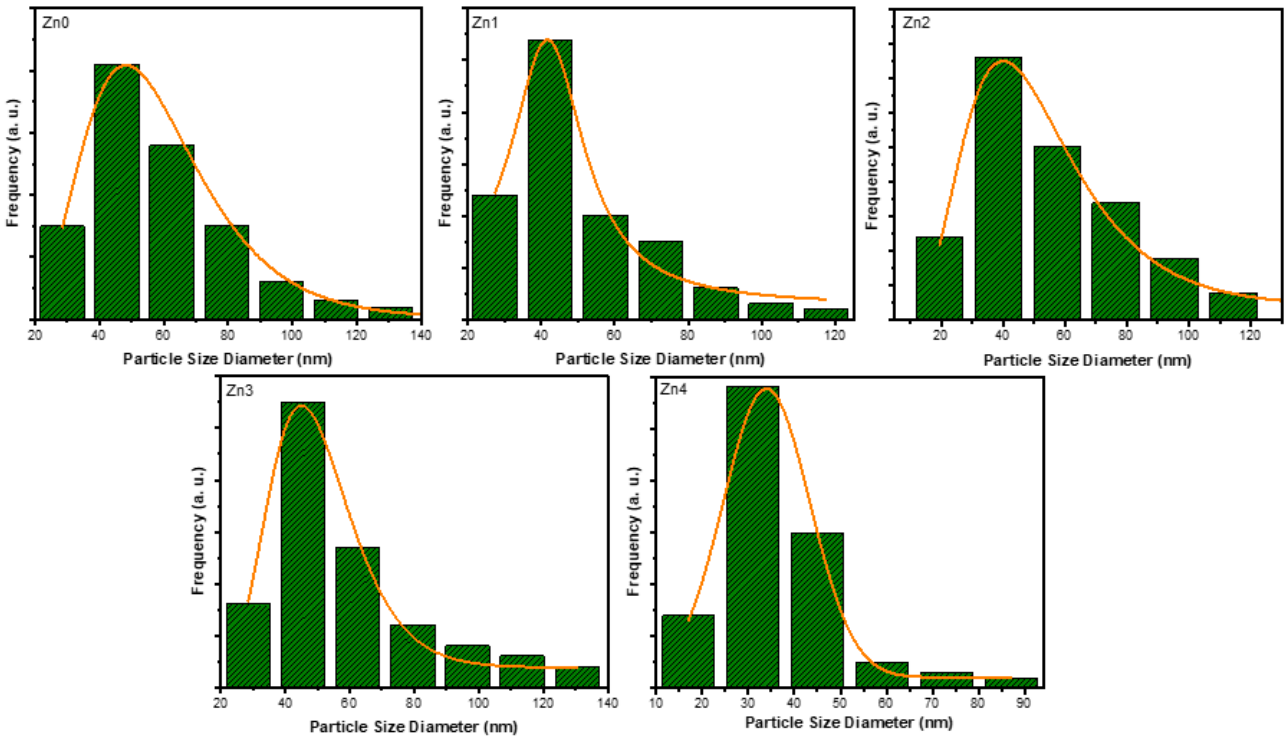

Fig. 4. Diameter size distribution of the Fe_2O_3/MWCNT/ZnO nanocomposites

The average diameter of the nanocomposites ranges between 33.97–55.19 nm, where the particles' diameter presents a similar trend as the increase of ZnO mass, from 48.00–48.56 nm. However, this value is lower than the ZnO sample, as showed in Figure Zn4 (Figure 4). The constituent compositions of the nanocomposite have also been characterized using EDX and the results are presented in Table 2. The developed nanocomposite is encompassed of Fe, C, Zn, and O, the primary elements of Fe_2O_3, MWCNT, and ZnO. The emergence of these elements has confirmed the successful synthesize of the nanocomposites. Interestingly, the Fe elements also experience a decrease following the increase of ZnO mass, confirmed by the increase of ZnO mass with the accelerated composition of the Zn element.

Table 2. Elemental composition of the Fe_2O_3/MWCNT/ZnO nanocomposites

Sample	Elements Composition (wt.%)			
	Fe	C	Zn	O
Zn0	63.91	08.15	-	27.94
Zn1	47.17	08.96	17.78	26.09
Zn2	33.49	05.57	33.49	26.39
Zn3	24.02	06.82	58.27	10.89
Zn4	-	-	82.96	17.04

The magnetic properties of Fe_2O_3/MWCNT/ZnO nanocomposites were characterized using VSM at room temperature and their results are represented by the hysteresis curves as sown in Figure 5. Figure 5 shows that the samples present weak ferromagnetic. This finding is linear with a study conducted by Shandilya, *et al*. [32]. The sample has saturation magnetization (*Ms*) of 0.37 emu/gram, much lower than a previous study that results in saturation magnetization of 4.26 emu/gram [33]. The result correlates with the addition of MWCNT that is a diamagnetic material, reducing the saturation magnetization of Fe_2O_3 [1]. Further, ZnO also carries diamagnetic characteristics, as proven by the curve representing negative saturation magnetization when exposed to a positive magnetic field [34].

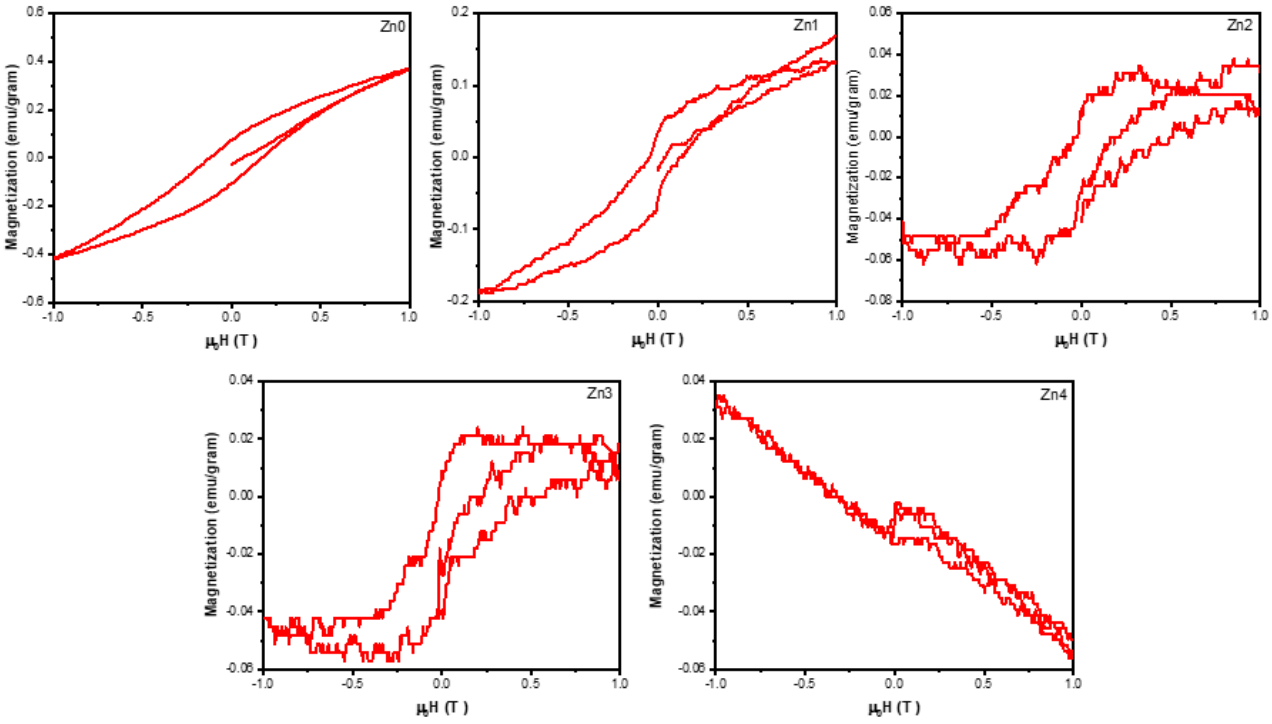

Fig. 5. Hysteresis curves of the Fe_2O_3/MWCNT/ZnO nanocomposites

The results of the qualitative analysis presented in Figure 5 show that the addition of ZnO nanoparticles reduces saturation magnetization value. The increase of ZnO nanoparticle causes an increase of diamagnetic material within the nanocomposite and reduce the ferromagnetic material, lowering the saturation magnetization. The details of the nanocomposite's magnetic parameters are shown in Table 3. Further, the decrease of saturation magnetization is caused by the expanded particle size after the addition of ZnO nanoparticles. The increase of particle size decreases surface to volume ratio, resulting in a lower contribution of surface spin toward the magnetic moment within the nanocomposite and reduced saturation magnetization [35]. Besides, the coercivity field (*Hc*) value tends to increase following the increase of ZnO composition, so that it has excellent application potential as storage and absorption for microwave (MAM).

Table 3. Magnetic parameters of the Fe_2O_3/MWCNT/ZnO nanocomposites

Sample	Magnetic Parameters		
	Ms **(emu/gram)**	***Mr*** **(emu/gram)**	***Hc*** **(T)**
Zn0	0.37	0.12	0.31
Zn1	0.17	0.08	0.23
Zn2	0.03	0.04	0.32
Zn3	0.01	0.02	0.39
Zn4	-	-	-

The optical properties of Fe_2O_3/MWCNT/ZnO nanocomposites are represented by the bandgap obtained from the calculation of UV-Vis characterization using Tauc plot direct transition method (Equation 1).

$$(\alpha h\upsilon) = A(h\upsilon - E_g)^2 \quad (1)$$

In which α is the absorption coefficient, A is the effective mass of the electron, h is the Planck's constant, and υ is the frequency [36]. The bandgap is an intercept obtained from the *x*-axis from the graph of the relationship between $h\upsilon$ and $(\alpha h\upsilon)^2$ (Figure 6). Figure 6 shows that the bandgap of Fe_2O_3 (Zn0) is 2.261 eV, which is close to the result of the previous study obtaining a bandgap of 2.200 eV [37]. Meanwhile, the gap energy of ZnO is 3.360 eV, confirming that the synthesized ZnO is a semiconductor. Additionally, the bandgap of the nanocomposites decreases following the increase of ZnO composition. It is caused by the bandgap value of the material that is inversely proportional to its particle size [38, 39].

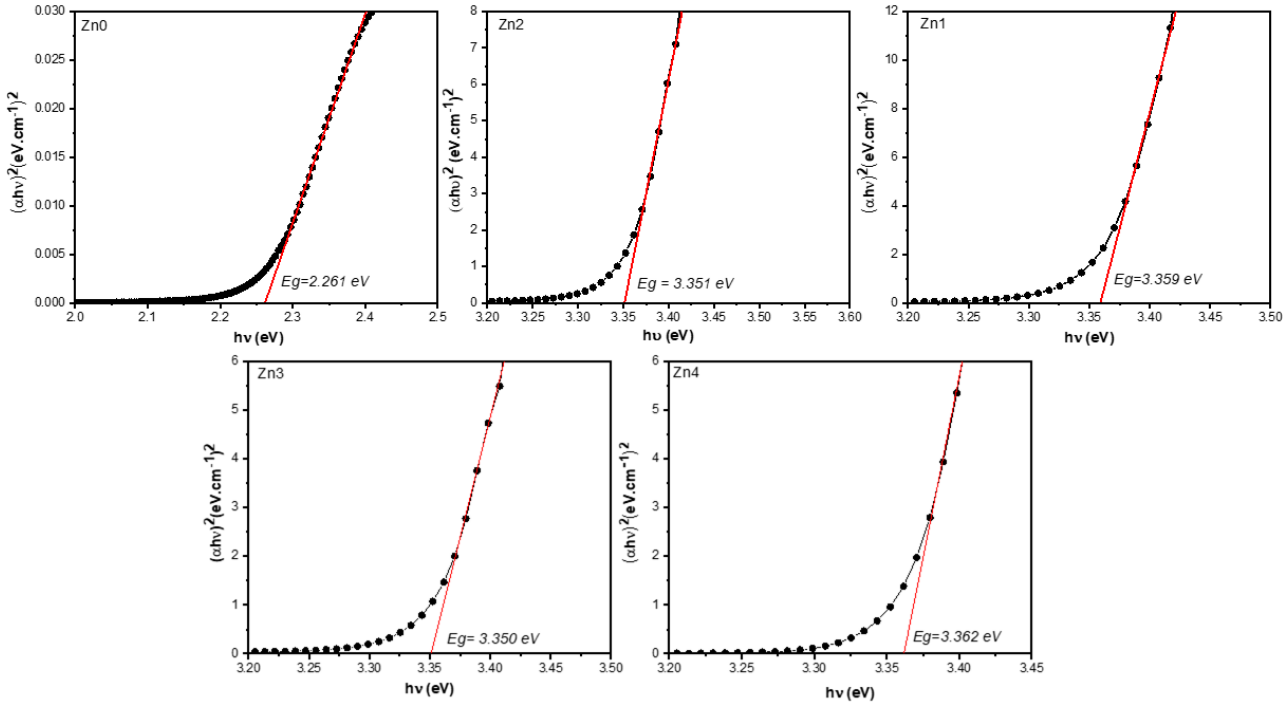

Fig. 6. Bandgap of the Fe_2O_3/MWCNT/ZnO nanocomposites

4. Conclusions

The Fe_2O_3/MWCNT/ZnO nanocomposites with a variation of ZnO composition were successfully fabricated using the precipitation method, as confirmed by the results of XRD and FTIR characterization. The obtained diffraction patterns of the nanocomposites validated the presence of Fe_2O_3 and ZnO phases, in which the ZnO peaks tended to increase following the increase of ZnO composition. Meanwhile, the presence of MWCNT was confirmed by the emergence of C=C bound vibration at wavenumbers of 1631–1640 cm^{-1}. The nanocomposite's morphology signified that the constituent particles were spherical, tube, and sheet, representing the presence of Fe_2O_3, MWCNT, and ZnO. Further, the nanocomposites presented saturation magnetization of 0.01–0.37 emu/gram with weak ferromagnetic characteristics. The bandgap of the nanocomposites was in the range of 2.261–3.360 eV.

References

[1] A. Taufiq *et al.*, "Eco-Friendly Fabrication of Fe_3O_4/MWCNT/ZnO Nanocomposites from Natural Sand for Radar Absorbing Materials," *International Journal of Nanoscience and Nanotechnology*, vol. 17, no. 1, pp. 41–53, Mar. 2021.
[2] R. Rahmawati *et al.*, "Preparation of MWCNT-Fe_3O_4 Nanocomposites from Iron Sand Using Sonochemical Route," *IOP Conference Series: Materials Science and Engineering*, vol. 202, p. 012013, May 2017, doi: 10.1088/1757-899X/202/1/012013.
[3] J. Nanosains, "Fabrikasi Material Nanokomposit Superkuat, Ringan dan Transparan Menggunakan Metode Simple Mixing," *Jurnal Nanosains & Nanoteknologi ISSN*, vol. 1979, p. 0880.
[4] ST. U. Intan Subadra *et al.*, "Preparation and Characterization of Magnetite Nanoparticles Combined with Polyaniline and Activated Carbon," *IOP Conference Series: Earth and Environmental Science*, vol. 276, p. 012041, Jun. 2019, doi: 10.1088/1755-1315/276/1/012041.
[5] A. Taufiq *et al.*, "Radar Absorption Performance of Fe_3O_4/AC/PANI Nanocomposites Prepared from Natural Iron Sand," *International Journal of Engineering*, vol. 33, no. 2, pp. 304–313, 2020.
[6] R. Rahmawati *et al.*, "The synthesis of Fe_3O_4/MWCNT nanocomposites from local iron sands for electrochemical sensors," in *AIP Conference Proceedings*, 2018, vol. 1958, p. 020016.
[7] A. G. Tamirat, J. Rick, A. A. Dubale, W.-N. Su, and B.-J. Hwang, "Using hematite for photoelectrochemical water splitting: a review of current progress and challenges," *Nanoscale Horizons*, vol. 1, no. 4, pp. 243–267, 2016.
[8] W. Wu *et al.*, "Large-scale and controlled synthesis of iron oxide magnetic short nanotubes: shape evolution, growth mechanism, and magnetic properties," *The Journal of Physical Chemistry C*, vol. 114, no. 39, pp. 16092–16103, 2010.
[9] H. Zhu, J. Deng, J. Chen, R. Yu, and X. Xing, "Growth of hematite nanowire arrays during dense pentlandite oxidation," *Journal of Materials Chemistry A*, vol. 2, no. 9, pp. 3008–3014, 2014.
[10] Y. Huang *et al.*, "Facile synthesis of α-Fe_2O_3 nanodisk with superior photocatalytic performance and mechanism insight," *Science and Technology of Advanced Materials*, vol. 16, no. 1, p. 014801, Feb. 2015, doi: 10.1088/1468-6996/16/1/014801.
[11] T. Lindgren, H. Wang, N. Beermann, L. Vayssieres, A. Hagfeldt, and S.-E. Lindquist, "Aqueous photoelectrochemistry of hematite nanorod array," *Solar Energy Materials and Solar Cells*, vol. 71, no. 2, pp. 231–243, Feb. 2002, doi: 10.1016/S0927-0248(01)00062-9.
[12] J. Chen, L. Xu, W. Li, and X. Gou, "α-Fe_2O_3 Nanotubes in Gas Sensor and Lithium-Ion Battery Applications," *Advanced Materials*, vol. 17, no. 5, pp. 582–586, 2005, doi: 10.1002/adma.200401101.
[13] J. H. Deng, K. P. Yu, and J. G. Xie, "Synthesis and Characteristics of Hierarchical Nanostructure Fe_3O_4 Coated Multi-Walled Carbon Nanotubes," *Advanced Materials Research*, vol. 926–930, pp. 258–261, 2014, doi: 10.4028/www.scientific.net/AMR.926-930.258.
[14] S. Y. Son, D. H. Lee, S. D. Kim, S. W. Sung, Y. S. Park, and J. H. Han, "Synthesis of multi-walled carbon nanotube in a gas-solid fluidized bed," *Korean Journal of Chemical Engineering*, vol. 23, no. 5, pp. 838–841, 2006.
[15] R. Xia *et al.*, "High-Frequency Absorption of the Hybrid Composites with Spindle-like Fe_3O_4 Nanoparticles and Multiwalled Carbon Nanotubes," *Nano*, vol. 11, no. 09, p. 1650097, 2016.
[16] M. A. Salam and R. Burk, "Synthesis and characterization of multi-walled carbon nanotubes modified with octadecylamine and polyethylene glycol," *Arabian Journal of Chemistry*, vol. 10, pp. S921–S927, Feb. 2017, doi: 10.1016/j.arabjc.2012.12.028.
[17] R. Leary and A. Westwood, "Carbonaceous nanomaterials for the enhancement of TiO_2 photocatalysis," *Carbon*, vol. 49, no. 3, pp. 741–772, Mar. 2011, doi: 10.1016/j.carbon.2010.10.010.
[18] V. S. Soplanit *et al.*, "Synthesis of Fe_3O_4/α-Fe_2O_3/ZnO nanocomposite for antibacterial application," Tangerang Selatan, Indonesia, 2020, p. 040031. doi: 10.1063/5.0002472.
[19] Kh. Ghanbari and A. Hajian, "Electrochemical characterization of Au/ZnO/PPy/RGO nanocomposite and its application for simultaneous determination of ascorbic acid, epinephrine, and uric acid," *Journal of Electroanalytical Chemistry*, vol. 801, pp. 466–479, Sep. 2017, doi: 10.1016/j.jelechem.2017.07.024.
[20] A. Taufiq *et al.*, "Effects of ZnO nanoparticles on the antifungal performance of Fe_3O_4/ZnO nanocomposites prepared from natural sand," *Advances in Natural Sciences: Nanoscience and Nanotechnology*, vol. 11, no. 4, p. 045004, Sep. 2020, doi: 10.1088/2043-6254/abb8c6.
[21] R. K. Matharu, L. Ciric, and M. Edirisinghe, "Nanocomposites: suitable alternatives as antimicrobial agents," *Nanotechnology*, vol. 29, no. 28, p. 282001, Jul. 2018, doi: 10.1088/1361-6528/aabbff.

[22] J. Jiang, J. Pi, and J. Cai, "The Advancing of Zinc Oxide Nanoparticles for Biomedical Applications," *Bioinorganic Chemistry and Applications*, vol. 2018, pp. 1–18, Jul. 2018, doi: 10.1155/2018/1062562.
[23] Q. Wu, Y. Si, Y.-Y. Wu, S.-W. Wang, G.-S. Wang, and L. Wang, "Fabrication and absorption properties based on ZnO nanocomposites adjusted by length–diameter ratio of ZnO nanorods," *CrystEngComm*, vol. 18, no. 22, pp. 4027–4031, May 2016, doi: 10.1039/C5CE02498F.
[24] A. Bauzá, T. J. Mooibroek, and A. Frontera, "Towards design strategies for anion–π interactions in crystal engineering," *CrystEngComm*, vol. 18, no. 1, pp. 10–23, 2016.
[25] Z. Wang, L. Wu, J. Zhou, Z. Jiang, and B. Shen, "Chemoselectivity-induced multiple interfaces in MWCNT/Fe_3O_4@ZnO heterotrimers for whole X-band microwave absorption," *Nanoscale*, vol. 6, no. 21, pp. 12298–12302, Jul. 2014, doi: 10.1039/C4NR03040K.
[26] A. Lassoued, B. Dkhil, A. Gadri, and S. Ammar, "Control of the shape and size of iron oxide (α-Fe_2O_3) nanoparticles synthesized through the chemical precipitation method," *Results in Physics*, vol. 7, pp. 3007–3015, Jan. 2017, doi: 10.1016/j.rinp.2017.07.066.
[27] M. Mohammadikish, "Hydrothermal synthesis, characterization and optical properties of ellipsoid shape α-Fe_2O_3 nanocrystals," *Ceramics International*, vol. 40, no. 1, Part B, pp. 1351–1358, Jan. 2014, doi: 10.1016/j.ceramint.2013.07.016.
[28] D. Sharma and R. Jha, "Transition metal (Co, Mn) co-doped ZnO nanoparticles: Effect on structural and optical properties," *Journal of Alloys and Compounds*, vol. 698, pp. 532–538, Mar. 2017, doi: 10.1016/j.jallcom.2016.12.227.
[29] T. Thirugnanam, "Effect of Polymers (PEG and PVP) on Sol-Gel Synthesis of Microsized Zinc Oxide," *Journal of Nanomaterials*, vol. 2013, pp. 1–7, 2013, doi: 10.1155/2013/362175.
[30] K. Saoud, R. Alsoubaihi, N. Bensalah, T. Bora, M. Bertino, and J. Dutta, "Synthesis of supported silver nano-spheres on zinc oxide nanorods for visible light photocatalytic applications," *Materials Research Bulletin*, vol. 63, pp. 134–140, Mar. 2015, doi: 10.1016/j.materresbull.2014.12.001.
[31] G. Xiong, U. Pal, J. G. Serrano, K. B. Ucer, and R. T. Williams, "Photoluminesence and FTIR study of ZnO nanoparticles: the impurity and defect perspective," *physica status solidi c*, vol. 3, no. 10, pp. 3577–3581, 2006.
[32] M. Shandilya, S. Thakur, and S. Thakur, "Magnetic amendment in the fabrication of environment friendly and biodegradable iron oxide/ethyl cellulose nanocomposite membrane via electrospinning," *Cellulose*, vol. 27, no. 17, pp. 10007–10017, Nov. 2020, doi: 10.1007/s10570-020-03455-5.
[33] M. Kargar, M. Ghashang, and M. R. Mohammad Shafiee, "Magnetic and Structural Characteristics of Fe_2O_3 Nanostructure Synthesized in the Presence of Sour Cherry Juice," *Journal of Advanced Materials and Processing*, vol. 4, no. 3, pp. 22–32, Sep. 2016.
[34] E. P. Etape, J. Foba-Tendo, L. J. Ngolui, B. V. Namondo, F. C. Yollande, and M. B. N. Nguimezong, "Structural Characterization and Magnetic Properties of Undoped and Ti-Doped ZnO Nanoparticles Prepared by Modified Oxalate Route," *Journal of Nanomaterials*, vol. 2018, pp. 1–9, 2018, doi: 10.1155/2018/9072325.
[35] P. Kaur *et al.*, "Tuning ferromagnetism in zinc oxide nanoparticles by chromium doping," *Applied Nanoscience*, vol. 5, no. 8, pp. 975–981, Nov. 2015, doi: 10.1007/s13204-014-0394-2.
[36] M. M. Rahman, M. M. Hussain, and A. M. Asiri, "Fabrication of 3-methoxyphenol sensor based on Fe_3O_4 decorated carbon nanotube nanocomposites for environmental safety: Real sample analyses," *PLOS ONE*, vol. 12, no. 9, p. e0177817, Sep. 2017, doi: 10.1371/journal.pone.0177817.
[37] A. A. Ismail, A. M. Ali, F. A. Harraz, M. Faisal, H. Shoukry, and A. E. Al-Salami, "A Facile Synthesis of alpha-Fe_2O_3/Carbon Nanotubes and Their Photocatalytic and Electrochemical Sensing Performances," *Int. J. Electrochem. Sci*, vol. 14, pp. 15–32, 2019.
[38] H. El Ghandoor, H. M. Zidan, M. M. Khalil, and M. I. M. Ismail, "Synthesis and some physical properties of magnetite (Fe_3O_4) nanoparticles," *Int. J. Electrochem. Sci*, vol. 7, no. 6, pp. 5734–5745, 2012.
[39] Y. Bagbi, A. Sarswat, D. Mohan, A. Pandey, and P. R. Solanki, "Lead (Pb 2+) adsorption by monodispersed magnetite nanoparticles: Surface analysis and effects of solution chemistry," *Journal of Environmental Chemical Engineering*, vol. 4, no. 4, pp. 4237–4247, Dec. 2016, doi: 10.1016/j.jece.2016.09.026.